



The Splash without a Merger

João A. S. Amarante^{1,2} , Leandro Beraldo e Silva³ , Victor P. Debattista³ , and Martin C. Smith¹¹ Key Laboratory of Galaxies and Cosmology, Shanghai Astronomical Observatory, Chinese Academy of Sciences, 80 Nandan Road, Shanghai 200030, People's Republic of China; joaoant@gmail.com² University of Chinese Academy of Sciences, No.19A Yuquan Road, Beijing 100049, People's Republic of China
³ Jeremiah Horrocks Institute, University of Central Lancashire, Preston PR1 2HE, UK

Received 2019 November 6; revised 2020 February 12; accepted 2020 February 21; published 2020 March 9

Abstract

The Milky Way's progenitor experienced several merger events that left their imprints on the stellar halo, including the *Gaia*-Sausage/Enceladus. Recently, it has been proposed that this event perturbed the proto-disk and gave rise to a metal-rich ($[\text{Fe}/\text{H}] > -1$), low angular momentum ($v_\phi < 100 \text{ km s}^{-1}$) stellar population. These stars have dynamical and chemical properties different from the accreted stellar halo, but are continuous with the canonical thick disk. In this Letter, we use a hydrodynamical simulation of an isolated galaxy that develops clumps that produce a bimodal thin+thick disk chemistry to explore whether it forms such a population. We demonstrate that clump scattering forms a metal-rich, low angular momentum population, without the need for a major merger. We show that, in the simulation, these stars have chemistry, kinematics, and density distribution in good agreement with those in the Milky Way.

Unified Astronomy Thesaurus concepts: Milky Way dynamics (1051); Milky Way formation (1053); Hydrodynamical simulations (767); Milky Way evolution (1052)

1. Introduction

Selecting a pure sample of stars in either the stellar halo or in the thick disk in the solar neighborhood is complicated by their significant overlap in both their velocity and metallicity distributions. A common approach for selecting local stellar halo stars uses a kinematic cut to select high transverse velocity stars. By selecting stars with $v_t > 200 \text{ km s}^{-1}$, one expects a negligible contamination by thick-disk stars. However, with the high-quality data provided by *Gaia* (Gaia Collaboration et al. 2016, 2018b), recent studies have shown that such a kinematic cut still leaves a population of stars with thick-disk chemistry (Gaia Collaboration et al. 2018a; Haywood et al. 2018; Amarante et al. 2020). This imprint is also seen when different kinematic criteria are chosen (e.g., Helmi et al. 2018), challenging our understanding of the formation of the Milky Way's (MW) thick disk.

Furthermore, Di Matteo et al. (2019) and Amarante et al. (2020) found that many counter-rotating stars in the solar neighborhood are too metal-rich to be considered part of the accreted halo. In particular, Di Matteo et al. (2019) noted a low angular momentum population with thick-disk chemistry (see, e.g., their Figure 13) and proposed that the classical MW inner halo is actually composed of two stellar populations: (i) heated stars from the thick disk (referred to by them as the “Plume”), where the heating mechanism is associated with a major merger event named the *Gaia*-Sausage/Enceladus⁴ (Belokurov et al. 2018; Helmi et al. 2018); (ii) accreted stars from the *Gaia*-Sausage.

Belokurov et al. (2019, hereafter B19), using the Sanders & Das (2018) catalog, disentangled the aforementioned low angular momentum structure from the canonical thick disk and stellar halo. They suggested that this structure, which they termed the Splash, is chemically and dynamically distinct from the known stellar populations in our Galaxy. Nonetheless, its formation must be linked to the thick disk as there is a smooth transition between the two populations in the kinematic-metallicity space. Moreover, they found Splash-like structures

in hydrodynamical simulations where the host galaxy underwent a major merger. Therefore they concluded the proto-galactic disk of the MW was likely heated during the *Gaia*-Sausage event about 10 Gyr ago, in agreement with other studies (e.g., Di Matteo et al. 2019; Gallart et al. 2019; Mackereth et al. 2019), and thereby formed the Splash. Finally, they argued that the thick-disk formation occurred before, during, and up to ~ 2 Gyr after the merger.

On the other hand, Clarke et al. (2019) presented a hydrodynamical simulation of an isolated galaxy that formed a thick disk purely via internal evolution driven by clump formation. These clumps dynamically heat the disk creating two chemically distinct disk components, with an overall double-exponential vertical profile (Beraldo e Silva et al. 2020), similar to the MW's thin and thick disks. They also showed that the model's clumps are similar to those observed in high-redshift galaxies. Therefore, a question that naturally arises is whether clumps are able to form stars with properties similar to the Splash, or whether the Splash stars uniquely need to form in a major merger event. In the following sections we demonstrate that clumps in the MW progenitor can produce stars with very similar kinematic and chemical properties as the observed Splash stars. This Letter is organized as follows: Sections 2 and 3 present the details of the simulated galaxy and show its dynamical and chemical features, respectively. Section 4 discusses the implications of our results.

2. Simulation

The simulation used in this Letter is described in detail in Clarke et al. (2019). The initial conditions are characterized by a spherical hot gas corona embedded in a dark matter halo with a Navarro–Frenk–White (Navarro et al. 1997) density profile with a virial radius $r_{200} \approx 200 \text{ kpc}$ and mass of $10^{12} M_\odot$. The gas has an initial net rotation and cools via metal-line cooling (Shen et al. 2010). It settles into a disk, and stars form wherever the temperature drops below 15,000 K and the density exceeds 1 cm^{-3} . Feedback by supernova explosions follows the

⁴ For short, we will just refer to it as the *Gaia*-Sausage.

blastwave implementation of Stinson et al. (2006), with thermal energy being injected to the interstellar medium with an efficiency of 10%. The feedback of asymptotic giant branch stars is also taken into account. Gas phase diffusion uses the method of Shen et al. (2010).

These initial conditions are self-consistently evolved for 10 Gyr with the smooth particle hydrodynamics+ N -body tree-code GASOLINE (Wadsley et al. 2004). As shown by Clarke et al. (2019), the metal-line cooling results in the formation of clumps during early times of the simulated galaxy. At the end of the simulation, the galaxy presents a chemical bimodality and geometric properties very similar to those observed for the MW (as shown by Beraldo e Silva et al. 2020). In particular, a thick disk, composed of old, α -rich stars is formed.⁵ This simulation evolves as an isolated galaxy, i.e., without any merger that could produce the metal-poor and high radial velocity dispersion population associated with the *Gaia*-Sausage observed for the MW (see Belokurov et al. 2018; Helmi et al. 2018) or any stellar halo component.

For comparison, we also ran another simulation from the same initial conditions and with the same procedure, except for the supernova feedback efficiency, which was set to 80%. This high feedback efficiency inhibits the formation of clumps and the simulation does not form a chemical or a geometric thick disk (Beraldo e Silva et al. 2020). We refer to this simulation as the non-clumpy simulation. This allows us to study the role of the clumps on the formation of the different populations in the simulation.

2.1. Simulated Solar Neighborhood

In order to reduce contamination from thin-disk stars, B19 selected stars in the region $0.5 < |z|/\text{kpc} < 3$. For reliable comparisons to their results, we apply a similar cut to the simulation data and define our mock solar neighborhood as all star-particles in the region $5 < R/\text{kpc} < 11$ and $|z| < 3$ kpc, where R is the cylindrical radius centered at the simulated galaxy center, and z is the height from the simulated galaxy plane. Unless explicitly mentioned, all our results are based on this geometrical slice. We have tested using the same $|z|$ range as B19 and the difference is the reduced amount of thin-disk star-particles. Nonetheless the trends between the simulated thick disk and Splash region discussed below are the same. Finally, throughout the Letter the velocities are given in cylindrical coordinates centered on the simulated galaxy center; v_R , v_ϕ , and v_z are positive in the direction of the galaxy center, galaxy rotation, and angular momentum vector, respectively.

3. Results

We now compare the kinematics and chemistry of the model to the results of B19. As described in Section 2, our simulation self-consistently evolves as an isolated galaxy and thus has no accreted stellar halo. Therefore, it has a lower fraction of metal-poor and of counter-rotating stars than the MW. For better comparison with the observational results, in most of our figures we adopt similar scales and color schemes as those used by B19. Moreover, whenever we use data from Sanders & Das (2018)⁶ we select stars with the same spatial selection, small

velocity errors ($\sigma_{v_\phi} < 20$ km s⁻¹), low [Fe/H] uncertainty ($\sigma_{[\text{Fe}/\text{H}]} < 0.15$), and accurate parallax ($\varpi/\sigma_\varpi > 5$) as in B19.

3.1. Chemistry-kinematics Features

Figure 1 (top row) shows the absolute density plot in the [Fe/H]– v_ϕ plane for both the MW (left) and the simulations (center and right). Each bin is divided by the total number of stars/star-particles following the selection criteria in the MW/simulations. As already discussed in B19, the MW has a significant amount of metal-rich ([Fe/H] > -1), low angular momentum ($v_\phi < 100$ km s⁻¹) stars (see, e.g., Nissen & Schuster 2010; Fernández-Alvar et al. 2019). The simulation with clumps also has a significant amount of such metal-rich low angular momentum stars, but lacks a significant amount of retrograde stars, mainly due to the absence of accreted stars,⁷ and has a slight overdensity at [Fe/H] > 0 and $v_\phi < 100$ km s⁻¹ compared to MW (but see B19 Figure 1, where, e.g., the left panels clearly show stars in this region). For comparison, the simulation without clumps, right panel, lacks a significant low angular momentum population.

The bottom row of Figure 1 shows the row-normalized density plot in the [Fe/H]– v_ϕ plane for both the MW (left) and simulations (center and right). This normalization has the advantage of enhancing the known velocity–metallicity correlation for both the thin and thick disk, where the former (*latter*) has a negative (*positive*) v_ϕ gradient with [Fe/H]. The red contours in the left panel indicate the different populations in the MW, as identified by B19, where the Splash is defined as the overdensity seen at the low angular momentum ($v_\phi \lesssim 80$ km s⁻¹) and relatively metal-rich ($-0.7 < [\text{Fe}/\text{H}] < -0.2$) region. The two known stellar halo overdensities, *Gaia*-Sausage (Belokurov et al. 2018; Helmi et al. 2018) and Sequoia (Barbá et al. 2019; Myeong et al. 2019), are also indicated. Although the Splash region is defined ad hoc in this plot, it is significantly different from the accreted stellar halo and the classical thick disk (defined as the α -rich disk; e.g., Bensby et al. 2003; Hayden et al. 2017) regions, as shown in B19 and later in this work.

The bottom middle panel of Figure 1 shows the results from the simulated clumpy galaxy. The same trends observed in the MW’s thin and thick disk are also observed here. In this panel, the red dashed lines are those defined by B19 with the MW data, while the green solid lines are defined from the simulation. The narrowness of the bands for the thin and thick disks in the simulation can be understood as being due to the absence of any observational errors. Nonetheless, the Splash region is exactly the same both in the MW and in the simulation. In the right panel, we show the same plot for the non-clumpy simulation. The solid and dashed red lines are the same as in the middle panel. The trends for the thin and thick disks are not as clear now and this galaxy can be described as having only one disk component (Clarke et al. 2019; Beraldo e Silva et al. 2020). Moreover, it lacks the low angular momentum ($v_\phi \lesssim 50$ km s⁻¹) star-particles of the Splash region.

Figure 2 shows the [Fe/H]– v_ϕ plane for the simulated MW analog color-coded according to different properties (see Figure 1 of B19 for comparison). The top left panel is color-coded by dispersion in v_R for each bin. As can be noted, the simulated

⁵ In the simulation, the $[\alpha/\text{Fe}]$ abundance is tracked by $[\text{O}/\text{Fe}]$.

⁶ http://www.ast.cam.ac.uk/~jls/data/gaia_spectro.hdf5

⁷ We note that not all retrograde stars with [Fe/H] > -1 observed in the MW are accreted.

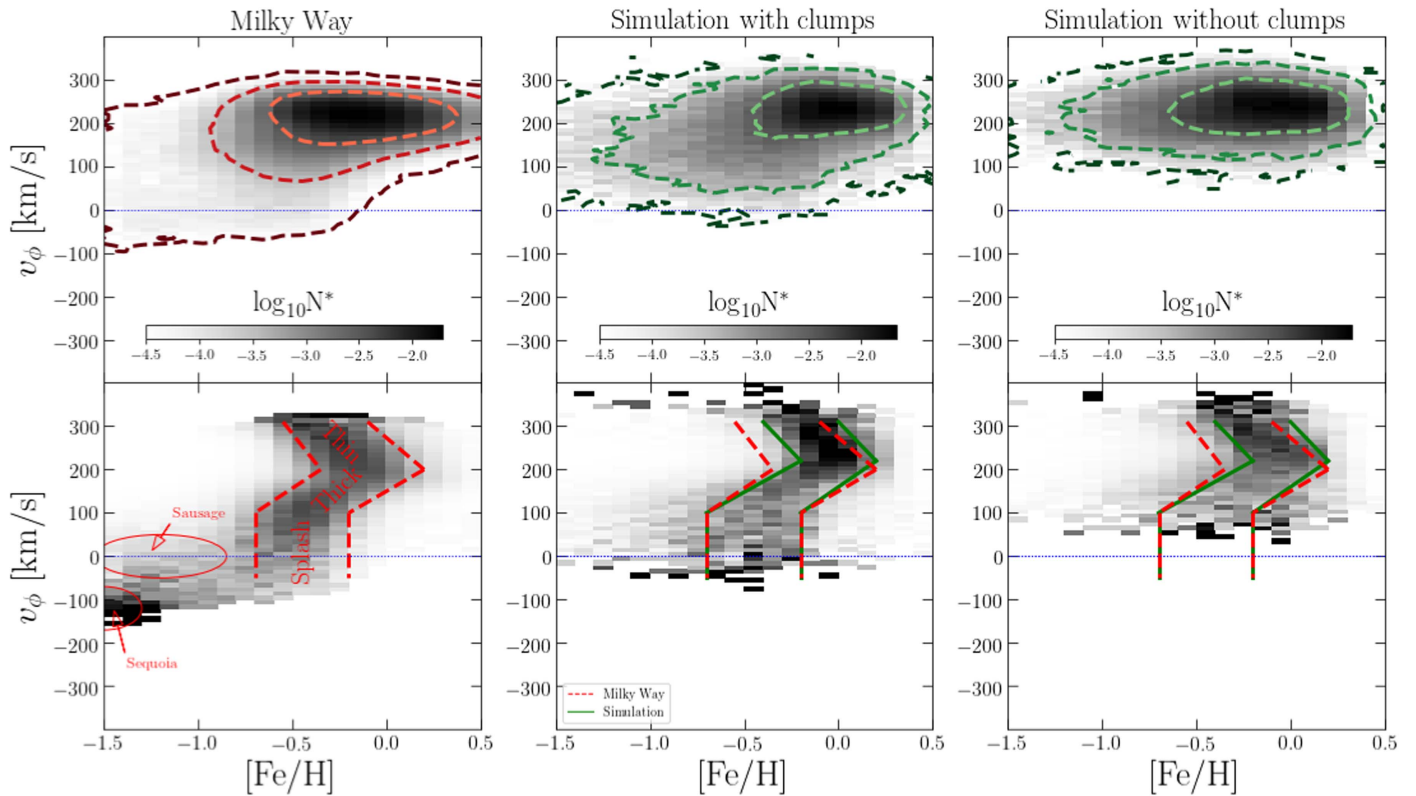


Figure 1. Left column shows the MW stars with $0.5 < |z|/\text{kpc} < 3$ from Sanders & Das (2018). The simulation panels are for stars with $5 < R/\text{kpc} < 11$ and $|z| < 3$ kpc; see details in the text. The middle and right columns show data from the clumpy and non-clumpy simulations, respectively. Top row: absolute density plots where each bin is divided by the total number of stars/star-particles following the selection criteria. The dashed lines are density contours on a logarithmic scale. Bottom row: row-normalized 2D density plot in the $[\text{Fe}/\text{H}]-v_\phi$ plane. The dashed red lines indicate the location of the thin disk, thick disk, and Splash, as defined by B19 in the observed data. The solid green lines show the equivalent regions in the clumpy simulation. The Splash region produced by the simulation is similar to that of the MW. Comparison of the central and right panels shows that the clumps are necessary to produce the Splash stars. Moreover, the simulation without clumps shows no Splash region in the velocity–metallicity plane. Finally, we also illustrate in the left panel the two known accreted stellar halo structures: *Gaia*-Sausage and Sequoia.

galaxy has the same trends as in the MW: the thin disk has a mild v_R dispersion and it smoothly increases from the thick disk toward the Splash region. As expected, the large v_R dispersion stars observed for $[\text{Fe}/\text{H}] < -0.7$, associated with the *Gaia*-Sausage and the Sequoia in the MW, are not present in our simulation as these stars were accreted. As in the MW, a similar trend is also observed for the dispersion in v_z ; see the top right panel. We stress that not only do trends match between the simulated galaxy and the observed data, but the velocity dispersion values are also very similar.

The bottom panels in Figure 2 show how the median age and $[\text{O}/\text{Fe}]$ vary in the $[\text{Fe}/\text{H}]-v_\phi$ plane. As in the MW, the thin disk region mostly comprises young stars and the disk gets older in its thick component. The oldest stars are located in the Splash region. The thin-disk region in our simulation is younger compared with the results in B19; as mentioned in Section 2, the simulation is evolved for only 10 Gyr and thus it will not reflect the same oldest ages as observed in the MW. Nonetheless, the thick disk and Splash region still have similar age gradients compared to the observations. Finally, the trends in $[\text{O}/\text{Fe}]$ are nicely matched to the $[\alpha/\text{Fe}]$ trends in the MW, where there is a smooth transition from slightly $[\text{O}/\text{Fe}]$ -rich for the thick disk to higher values in the Splash region.

Clarke et al. (2019) showed that, in the simulation, a small population of α -poor stars forms at the same time as the α -rich ones (indeed this is one of the key predictions of the model). We have verified that the publicly available APOGEE-*Gaia*

DR12 catalog⁸ indeed confirms that retrograde Splash stars are found both in the α -rich and α -poor in situ regions (as defined in Mackereth et al. 2019), supporting our conclusion that scattering by clumps can produce the counter-rotating Splash stars in the MW.

B19 analyzed LAMOST K giants (Luo et al. 2015) in order to verify how far from the plane the Splash stars are detected and to determine where the canonical thick-disk transitions to the Splash-dominated region. They found that at $|z| \sim 5$ kpc there is a sharp gradient in median v_ϕ where the low angular momentum Splash stars dominate for higher $|z|$ (see their Figure 8). Although the stellar density of the disk in our simulated galaxy decreases faster with $|z|$ compared with the MW’s disk, we are still able to verify the transition region, if any, in the simulation. The left panel in Figure 3 shows the stellar density in the $R-|z|$ plane for the simulation. The red and orange curves have the same velocity–metallicity intervals as in B19 and they are a rough representation of the canonical thin and thick disks, respectively. The black dashed curves outline the spatial extent of the Splash stars in our simulation. In order to avoid the tail of the stellar halo distribution, B19 restricted their velocity range to $-20 < v_\phi < 50 \text{ km s}^{-1}$. Even though our simulation does not have an accreted halo, we adopt the same range. We note that both in the simulation and in the MW, the Splash stars

⁸ https://www.sdss.org/dr12/irspec/spectro_data/

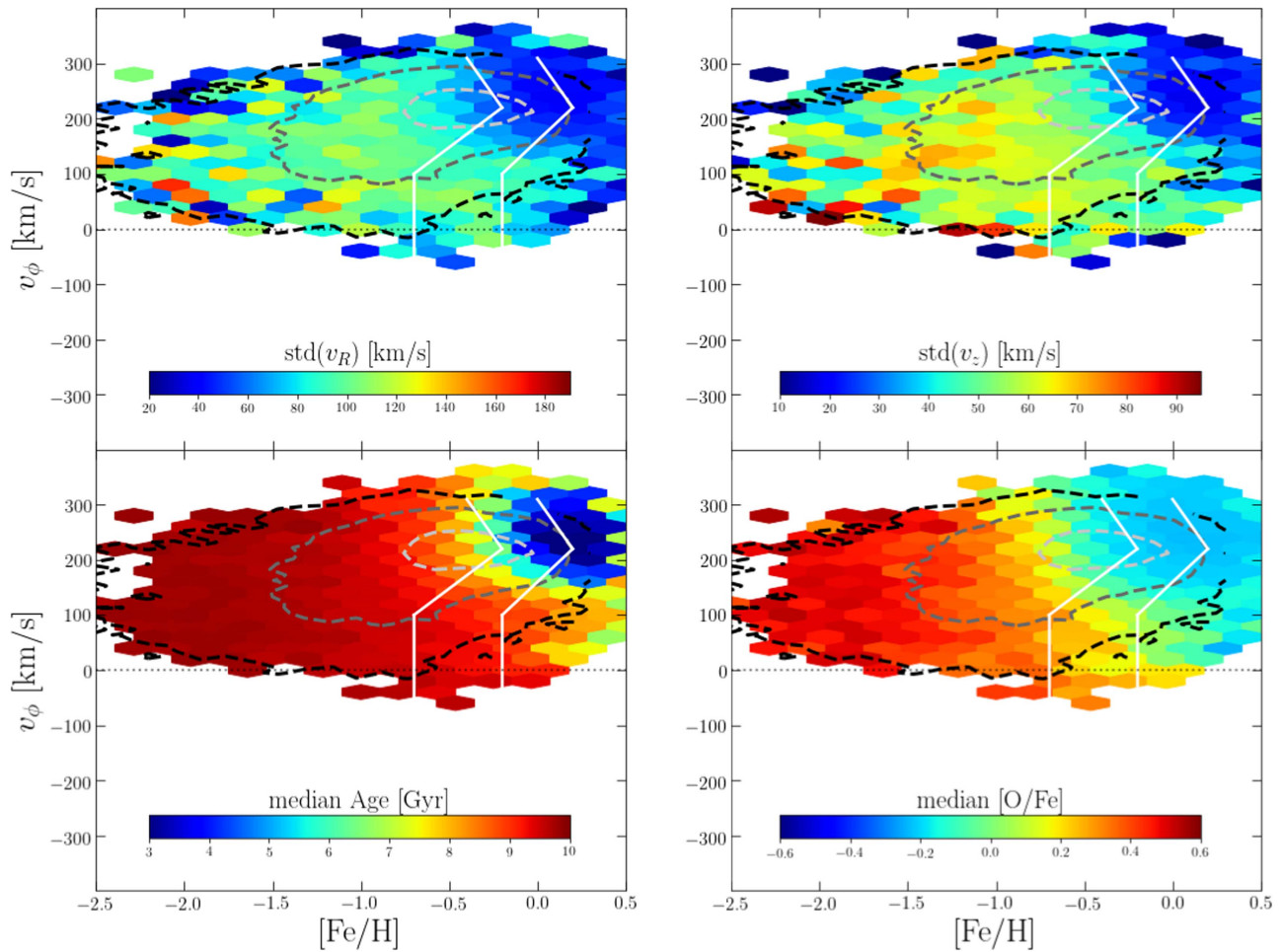


Figure 2. $[\text{Fe}/\text{H}]-v_\phi$ plane in the simulated clumpy galaxy, $5 < R/\text{kpc} < 11$ and $|z| < 3$ kpc, which was evolved for only 10 Gyr. The dashed lines are the density contours on a logarithmic scale. The solid white lines define the thin disk, thick disk, and Splash regions in the simulation as in Figure 1. Top row: on the left, color-coded by radial velocity dispersion, it is possible to see the transition from the thin disk population toward the thick disk going from mild to higher radial velocity dispersion. The Splash region has a higher radial velocity dispersion compared with the thick-disk counterpart. A similar trend is observed in the vertical velocity dispersion shown on the right. Bottom row: on the left we see that the Splash region is composed of the oldest stars in the simulation, whereas the thin disk is the youngest and the thick disk has intermediate to old stars. Finally on the right, the smooth $[\text{O}/\text{Fe}]$ transition from the thick region to the Splash region hints at their related origins.

extend up to $|z| \sim 10$ kpc and are also concentrated within $R \sim 10$ kpc.

The right panel of Figure 3 shows how the median v_ϕ changes in the $[\text{Fe}/\text{H}]-|z|$ plane. In the Splash metallicity range, defined by the two vertical dashed lines, we note two features similar to those observed in the MW: (i) the negative gradient of thick disk’s median v_ϕ with $|z|$; (ii) a transition at $|z| \sim 5$ kpc (horizontal dashed line) where the low angular momentum Splash stars start to dominate for larger heights. This reinforces the idea that internal dynamical processes in a clumpy proto-disk can also create Splash stars.

3.2. Simulated Splash Number Fraction

In this subsection, we estimate the Splash-like population in the simulation with clumps and compare with the MW. B19 estimated that in the range $2 < |z|/\text{kpc} < 3$ and $-0.7 < [\text{Fe}/\text{H}] < -0.2$ the Splash population dominates the tail of the v_ϕ distribution, i.e., $v_\phi < 100 \text{ km s}^{-1}$. The left panel of Figure 4 shows the cumulative distribution of v_ϕ for the MW (black) and simulation (red) in the aforementioned metallicity and spatial range: approximately 15% of the stars in the MW have $v_\phi < 100 \text{ km s}^{-1}$, whereas the simulation with clumps has

about 25% of star-particles in the same regime. However, if we scale v_ϕ by the median value for each distribution, the simulation with clumps has $\approx 20\%$ of star-particles in the equivalent low angular momentum tail, remarkably similar to the MW.

The right panel of Figure 4 shows the fraction of star-particles with halo kinematics in the simulation chemical thick disk. We used a spatial range similar to that used in Di Matteo et al. (2019). We also followed their criterion for halo kinematics, $\sqrt{(v_\phi - v_{\text{LSR}})^2 + v_R^2 + v_z^2} > 180 \text{ km s}^{-1}$, where $v_{\text{LSR}} = 233 \text{ km s}^{-1}$ and it is the velocity at the local standard of rest in the simulation (Clarke et al. 2019). The separation criterion between the thin and thick disks for the simulations follows Clarke et al. (2019). We observe that the simulation follows the same trends as in the MW (see Figure 18 in Di Matteo et al. 2019): (i) the fraction of halo-like kinematics is $\approx 25\%$ in the range where the Splash stars are concentrated; (ii) this fraction drops quickly as the metallicity increases. The larger fraction of halo-kinematics stars at $[\text{Fe}/\text{H}] > -0.2$ in the simulation, compared with the MW, can be due to differences in the details of the later star formation history and/or the selection function of the APOGEE data.

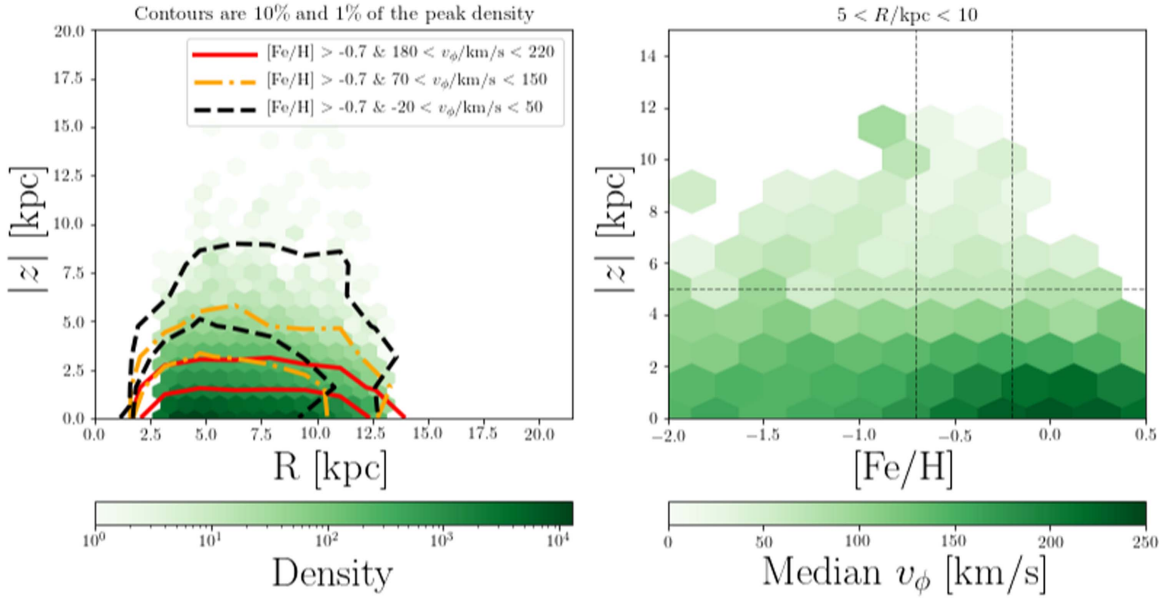


Figure 3. Spatial extent of the Splash stars in the simulation. The left plot shows the distribution of the metal-rich stars for three different velocity ranges. The thin and thick-disk-like stars are indicated by the red and orange curves, respectively. The curves are the contours of 10% and 1% of the peak density. The lower angular momentum stars (dashed black curves) represent the Splash stars and have similar $|z|$ extension in comparison to observations (see B19, Figure 8). On the right, we show the $[Fe/H]$ - $|z|$ plane color-coded by median v_ϕ . The trends are also remarkably similar to the observations; the transition between the canonical thick disk to the Splash-dominated region also occurs at $|z| \sim 5$ kpc.

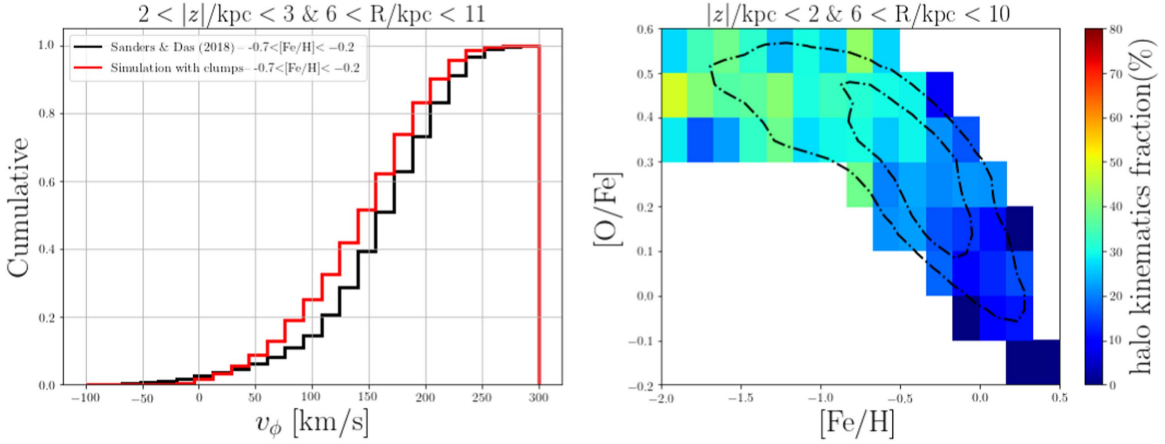


Figure 4. Left panel: the cumulative v_ϕ distribution for the MW (black) and simulation with clumps (red) in the Splash metallicity regime, $-0.7 < [Fe/H] < -0.2$. The fractions of stars and star-particles in the tail of the distribution are $\approx 15\%$ and $\approx 25\%$, respectively. Right panel: an estimate of the fraction of star-particles with halo-like kinematics, $\sqrt{(v_\phi - v_{\text{LSR}})^2 + v_R^2 + v_z^2} > 180 \text{ km s}^{-1}$, following the criteria from Di Matteo et al. (2019, see their Figure 18 for a comparison with the MW). We show the fractions for the chemically defined thick disk in the simulation (Clarke et al. 2019). The black curves are the contours of 50% and 10% of the peak density. The trends in the simulation with clumps are very similar to the MW; see the text for details.

3.3. The Age of Simulated Splash Stars

In order to compare the age difference between the accreted halo and the Splash stars, B19 analyzed the age distribution of the counter-rotating stars for two distinct metallicity ranges (see their Figure 4). The metal-poor ($[Fe/H] < -0.7$) region, corresponding to the accreted halo has a peak at ~ 12.5 Gyr⁹ and a sharp drop at ~ 10 Gyr. On the other hand, the age distribution for the Splash stars, $-0.7 < [Fe/H] < -0.2$, has a slightly younger peak at ~ 11.5 Gyr and also a sharp drop at ~ 10 Gyr ($\sim 30\%$ of these stars are younger than 10 Gyr). They propose that the Splash is made up of stars from the Galaxy’s proto-disk whose orbits were heated by the *Gaia*-Sausage

accretion event. Moreover, the star formation for the Splash stars ceased just after the merger, i.e., around 9.5 Gyr ago.

In the left panel of Figure 5, we show the age distribution in our simulation using the same velocity–metallicity interval as in B19. As already mentioned, our oldest age is 10 Gyr and the fact there is no shift between the metal-poor (blue) and Splash stars (black) curves merely reflects that our simulation represents an isolated galaxy with no old accreted stellar halo. Nonetheless, it is evident that the counter-rotating stars in the simulation are also old and cease to form after 3 Gyr. This fact is qualitatively similar to what is observed in the MW. The red curve in this panel corresponds to the canonical thin+thick distribution, $v_\phi > 200 \text{ km s}^{-1}$ and $[Fe/H] > -0.7$. As expected it extends over the full age range in the simulated galaxy in agreement with the observed data. Finally, the green

⁹ Their ages are limited to 12.5 Gyr.

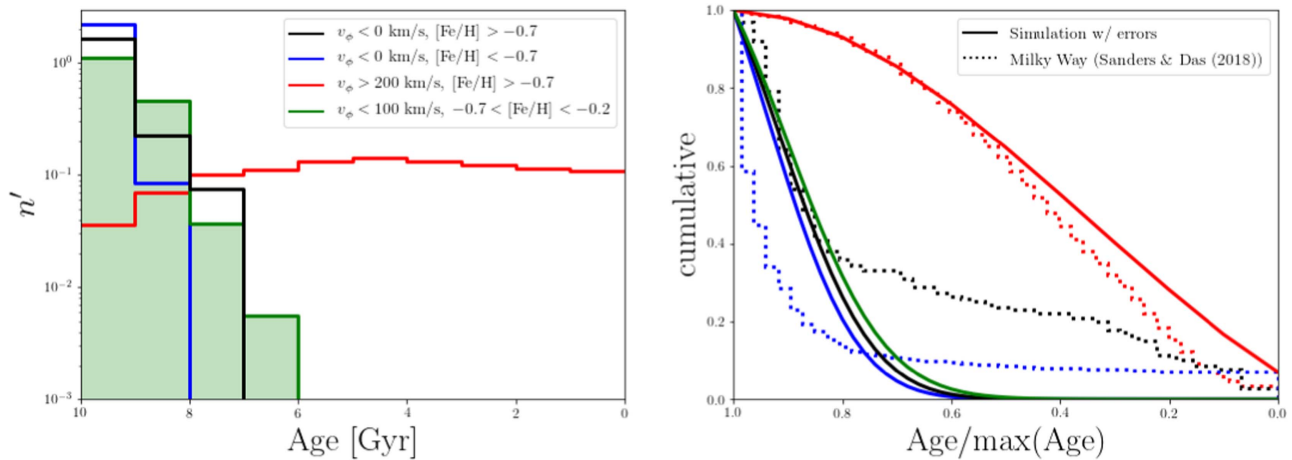


Figure 5. Left panel: error-free age distribution for the simulated stars in the simulated clumpy galaxy with $5 < R/\text{kpc} < 11$ and $|z| < 3$ kpc. n' is the probability density function of each 1 Gyr age bin. The black and blue curves show the counter-rotating stars for metal-rich and metal-poor intervals, respectively. All the counter-rotating stars in the simulation are older than 7 Gyr. The absence of the shift in the peak of the age distribution between the two curves, seen by B19, reflects the fact that our simulation has no accreted halo. The red curve shows the age distribution of the classical thin+thick disk in the simulation, which was only evolved for 10 Gyr. The green shaded area corresponds to the age distribution of the simulation Splash region defined in Figure 1. As it includes stars with $v_\phi < 100$ km s $^{-1}$, some thick-disk stars are present. Right panel: cumulative age distribution for the MW (dotted lines) and simulation (solid lines) convolved with observational errors. The colors correspond to the same velocity and $[\text{Fe}/\text{H}]$ interval as in the left panel. We divide each age by the maximum age in the MW data (12.5 Gyr) and the simulation (10 Gyr).

shaded area is the age distribution for the Splash stars defined as in Figure 1, i.e., $v_\phi < 100$ km s $^{-1}$ and $-0.7 < [\text{Fe}/\text{H}] < -0.2$. Now, the age extends to an extra 1 Gyr, due to the contamination of thick disk, i.e., α -rich stars. As shown by Clarke et al. (2019), all the star-particles in the simulation thick disk are older than 6 Gyr. Therefore, our result reinforces the connection between the thick disk and the Splash stars, where the latter could naturally exist in galaxies with a disk dichotomy.

Figure 5 (right panel) shows the cumulative distribution for the MW (dotted lines) and the simulation (solid lines) convolved with the median error from the observational data (median $\sigma_{\text{age}} \approx 1.3$ Gyr).¹⁰ For a better comparison, we divided the age intervals by the maximum age in the simulation (10 Gyr) and observation (12.5 Gyr). For $v_\phi < 0$ and $[\text{Fe}/\text{H}] > -0.7$ the MW (black dotted line) has a truncated star formation history characterized by: (i) approximately 60% of stars are older than $\text{age}/\text{max}(\text{age}) \approx 0.8$, (ii) an extended tail toward young ages. B19 associated the truncation with the cessation of the MW’s disk heating during the *Gaia*-Sausage merger. Similarly to the MW, the simulation also has approximately 60% of stars older than $\text{age}/\text{max}(\text{age}) \approx 0.8$ (black and green solid lines). The lack of young Splash-like stars in the simulation is explained by the fact that the clumps, which are responsible for producing the Splash, stop forming after 4 Gyr. The difference between the simulation and the MW, in terms of the extended tail of ages, only happens after both the clumps and the *Gaia*-Sausage are completed. We also note, by analyzing the simulation snapshots, that this old population is already kinematically hot in the first 3 Gyr of the simulation. Therefore, internal dynamical heating in a MW-like galaxy is enough to heat the primordial disk in its early stages and produce a kinematically hot population with $v_\phi < 100$ km s $^{-1}$, as shown by the green distribution in Figure 5.

4. Conclusions

Di Matteo et al. (2019) suggested that the Splash stars (which they refer to as the “Plume”) represent the low angular momentum tail of the thick disk and therefore it is not a distinct component from the MW. On the other hand, B19 argue on the necessity of three components (thin disk, thick disk, and Splash) to explain the v_ϕ distribution for $-0.7 < [\text{Fe}/\text{H}] < -0.2$ and $2 < |z|/\text{kpc} < 3$. Based on their age distribution, they also suggest that the Splash formed only in the early times of the MW, whereas the thick disk had a continuous formation over time.

From B19’s work the existence of four distinct stellar populations in the dynamical-chemical space is suggested: thin disk, thick disk, accreted halo, and the Splash, the latter sometimes being referred to as the in situ halo. The origin of the Splash also relates to the thick disk and it possibly contains the first stars in the proto-disk of our Galaxy’s progenitor. Besides that, there is clear evidence of a major merger event that occurred in the early stages of the MW (e.g., Helmi 2008; Belokurov et al. 2018; Haywood et al. 2018; Di Matteo et al. 2019). Di Matteo et al. (2019) and B19 proposed that this merger event could have excited the proto-disk and given rise to the low angular momentum, high radial velocity dispersion, and relatively metal-rich Splash stars.

In this Letter we analyzed an isolated galaxy simulation in order to investigate the formation of Splash stars. We showed that a clumpy MW analog can naturally form not just the chemical and geometric thin and thick disks (Clarke et al. 2019; Beraldo e Silva et al. 2020), but also the Splash, with distribution, kinematics, and chemistry similar to those observed in our Galaxy. This is a new scenario for the formation of the Splash, as in our case there was no accretion event and therefore no accreted stellar halo. Moreover, in this scenario, the formation of the Splash stars occurs in the simulation’s first Gyr. The thick disk and Splash population have a common origin, where the latter is the low angular momentum tail of the former, as initially suggested by Di Matteo et al. (2019). This is due to the smooth transition in

¹⁰ We select stars in Sanders & Das (2018) with estimated ages error lower than 2 Gyr.

kinematics, age, and [O/Fe] between the thick-disk and Splash regions seen in Figure 2. We also show that a similar simulation without clumps fails to reproduce the low rotational velocity patterns of the MW. We verified that the simulated Splash has a similar number fraction (Section 3.2) and age trends (Section 3.3) as observed in the MW. Our results suggest that a Splash population is expected in any galaxy that underwent a clumpy star formation episode.

Finally, we note that the two different formation scenarios for the Splash population, i.e., clumpy star formation (this work) or a major merger (Belokurov et al. 2019; Di Matteo et al. 2019), are not mutually exclusive, since clumps can have an ex situ origin associated to mergers (e.g., Mandelker et al. 2014). The effect of the merger on the disk depends on several parameters, such as the initial gas fraction and orbit (see, e.g., Di Matteo et al. 2011). Moreover, the proximity of the satellite’s disruption, whether close or far from the disk, also plays an important role on the disk heating (Sellwood et al. 1998), and requires further study for the *Gaia*-Sausage.

The authors wish to thank the anonymous referee for useful comments that helped improve this work. J.A. and M.C.S. acknowledge support from the National Key Basic Research and Development Program of China (No. 2018YFA0404501) and NSFC grant 11673083. J.A. also acknowledges The World Academy of Sciences and the Chinese Academy of Sciences for the CAS-TWAS fellowship. J.A. is also grateful for the hospitality of Jeremiah Horrocks Institute at UCLan during his visit. V.P.D. and L.B.S. are supported by STFC Consolidated grant #ST/R000786/1. The simulations in this Letter were run at the DiRAC Shared Memory Processing system at the University of Cambridge, operated by the COSMOS Project at the Department of Applied Mathematics and Theoretical Physics on behalf of the STFC DiRAC HPC Facility (www.dirac.ac.uk). This equipment was funded by BIS National E-infrastructure capital grant ST/J005673/1, STFC capital grant ST/H008586/1, and STFC DiRAC Operations grant ST/K00333X/1. DiRAC is part of the National E-Infrastructure.

ORCID iDs

João A. S. Amarante  <https://orcid.org/0000-0002-7662-5475>

Leandro Beraldo e Silva  <https://orcid.org/0000-0002-0740-1507>

Victor P. Debattista  <https://orcid.org/0000-0001-7902-0116>

References

- Amarante, J. A. S., Smith, M. C., & Boeche, C. 2020, MNRAS, 492, 3816
 Barbá, R. H., Minniti, D., Geisler, D., et al. 2019, ApJL, 870, L24
 Belokurov, V., Erkal, D., Evans, N. W., Koposov, S. E., & Deason, A. J. 2018, MNRAS, 478, 611
 Belokurov, V., Sanders, J. L., Fattahi, A., et al. 2019, arXiv:1909.04679
 Bensby, T., Feltzing, S., & Lundström, I. 2003, A&A, 410, 527
 Beraldo e Silva, L., Debattista, V. P., Khachaturyants, T., & Nidever, D. 2020, MNRAS, 492, 4716
 Clarke, A. J., Debattista, V. P., Nidever, D. L., et al. 2019, MNRAS, 484, 3476
 Di Matteo, P., Haywood, M., Lehnert, M. D., et al. 2019, A&A, 632, A4
 Di Matteo, P., Lehnert, M. D., Qu, Y., & van Driel, W. 2011, A&A, 525, L3
 Fernández-Alvar, E., Fernández-Trincado, J. G., Moreno, E., et al. 2019, MNRAS, 487, 1462
 Gaia Collaboration, Babusiaux, C., van Leeuwen, F., et al. 2018a, A&A, 616, A10
 Gaia Collaboration, Brown, A. G. A., Vallenari, A., et al. 2018b, A&A, 616, A1
 Gaia Collaboration, Prusti, T., de Bruijne, J. H. J., et al. 2016, A&A, 595, A1
 Gallart, C., Bernard, E. J., Brook, C. B., et al. 2019, NatAs, 3, 932
 Hayden, M. R., Recio-Blanco, A., de Laverny, P., Mikolaitis, S., & Worley, C. C. 2017, A&A, 608, L1
 Haywood, M., Di Matteo, P., Lehnert, M. D., et al. 2018, ApJ, 863, 113
 Helmi, A. 2008, A&ARv, 15, 145
 Helmi, A., Babusiaux, C., Koppelman, H. H., et al. 2018, Natur, 563, 85
 Luo, A. L., Zhao, Y.-H., Zhao, G., et al. 2015, RAA, 15, 1095
 Mackereth, J. T., Schiavon, R. P., Pfeffer, J., et al. 2019, MNRAS, 482, 3426
 Mandelker, N., Dekel, A., Ceverino, D., et al. 2014, MNRAS, 443, 3675
 Myeong, G. C., Vasiliev, E., Iorio, G., Evans, N. W., & Belokurov, V. 2019, MNRAS, 488, 1235
 Navarro, J. F., Frenk, C. S., & White, S. D. M. 1997, ApJ, 490, 493
 Nissen, P. E., & Schuster, W. J. 2010, A&A, 511, L10
 Sanders, J. L., & Das, P. 2018, MNRAS, 481, 4093
 Sellwood, J. A., Nelson, R. W., & Tremaine, S. 1998, ApJ, 506, 590
 Shen, S., Wadsley, J., & Stinson, G. 2010, MNRAS, 407, 1581
 Stinson, G., Seth, A., Katz, N., et al. 2006, MNRAS, 373, 1074
 Wadsley, J., Stadel, J., & Quinn, T. 2004, NewA, 9, 137